INTECH
open science | open minds

OPEN ACCESS
ARTICLE

Nanomaterials and Nanotechnology

A New Approach to the Habit Determination of Nano-objects by SEM

Regular Paper

K. S. Maksimov[1,*] and S. K. Maksimov[1]

1 Moscow Institute of Electronic Technology (Technical University), Zelenograd, Moscow region, Russia
* Corresponding author E-mail: Cyril@pisem.net

Received 2 April 2013; Accepted 21 May 2013

Abstract A novel approach to the inspection of nanoparticle habit was proposed in our previous papers. This approach is based on a joint analysis of two scanning electron microscopy (SEM) images corresponding to different convergences of illuminating electron beams. However, increasing convergence worsens an image as the result of spherical aberration. Therefore, for the first time in this paper we describe in detail a new approach which is an alternative to the method of two convergences. It is based on the use of two defocusings which are identical in size, but opposite in signs, thereby. simplifying the demands of SEM.

Keywords Nano-Object Size, Nano-Object Shape, Scanning Electron Microscopy, Convergent Illuminating Electron Beams, Defocused Images

1. Introduction

The problem of nanoparticle characterization is still a significant one in nanotechnologies. It is especially important for pharmacology and medicine. Particles can be vehicles for drugs in given points of an organism, but their percolation through membranes depends on their structure and shape (habit). Particles can stimulate desirable and undesirable (even fatal dangerous) variations of metabolism and these processes depend also on their structural-morphological characteristics. Nanoparticles could be used as catalysts in technologies for the manufacture of drugs or as substances for encapsulation of non-persistent medicines. Many substances which can be used as medicines are water-insoluble, yet their digestion in an organism is required; therefore, their nanodimensional forms are assimilated more easily. Nanocrystallization can then be a principal approach in pharmacology, providing the creation of new medicines in essence [1–3]. It is imperative that we utilize the vast opportunities that are provided by the use of nanoparticles and, therefore, the nanoparticle industry should certainly be developed.

2. The problem of size characterization of nano-objects

The rapid progress made in modern nanotechnologies has escalated the problem of precise and ultra-precise size measurements. The semimetal–semiconductor phase transition occurs in Bi nanowires with a diameter of 48 nm [4]. The transition to the superparamagnetic state is suppressed in Ni wires with a diameter of 35 nm [5] and in Co nanowires with a diameter of 14 nm [6]. The influence of quantum

effects caused by excitons is observed in InP wires with a diameter of less than 20 nm [7]. When the size of ZrO_2 particles changes from 3.7 to 29.5 nm, three structural modifications arise and several changes in equilibrium habits occur [8]. However, even precise measurements of average sizes do not solve the problem of characterization of a nano-object. First, properties of nano-objects are anisotropic, the objects themselves can have a complex shape and an adequate explanation of their properties requires the knowledge of their sizes along different crystallographic directions. Second, in order to ensure ecological safety, it is necessary to determine the habit of nanoparticles and the relevant numerical characteristics, i.e., relative fractions of faces of different types [9–11].

A spatial resolution that makes it possible to solve metrological problems for nano-objects is provided by scanning probe methods, transmission electron microscopy and SEM [10, 11]. Scanning probe methods enable one to measure details of a relief several tens of nanometres in height (for example, arrays of quantum dots) with an Ångström accuracy, and to determine the shape of nano-objects or etch figures. The efficiency of scanning probe methods, which is required to control devices with larger areas of the location of nano-objects, can be increased using multicantilever systems. However, the problems associated with the low velocity of mechanical scanning, inhomogeneities of nano-objects in height and distribution, the necessity of determining the crystal structure and orientation of the objects, large aspect ratios and slopes of lateral faces [12] have not been overcome to date. Exhaustive information on the structural and morphological characteristics of nano-objects has been obtained using transmission electron microscopy with a spatial resolution of approximately 0.15 nm on instruments operating in static and scanning image modes. Transmission electron microscopy makes it possible to determine the crystallographic characteristics of nano-objects and to examine their habit with the use of stereomicroscopy [13]. High-resolution electron microscopy methods ensure an Ångström accuracy of measurements [11, 14]. However, although transmission electron microscopy is a promising method for characterizing arrays of nano-objects [11], its limiting resolution is suited only for layers with a thickness close to or less than 10 nm, which, in turn, has limited its application to objects with a relief height ≥ 10 nm [14]. In a number of cases, the interpretation of nano-object images invites theoretical investigation of the contrast [14–15]. This requires that the operators have the highest level of skill. Therefore, the solution to metrological problems in nanotechnologies necessitates the use of alternative approaches, which, at the present time, can be based only on SEM techniques.

3. Traditional and untraditional approaches to the size characterization of nano-objects by scanning electron microscopy

The formation of SEM images includes two stages. In the first stage, which is based on the use of the wave properties of electrons, the formation of an electron probe occurs in accordance with the laws of electron optics. In the second stage, which is based on the use of the corpuscular properties of electrons, a particle releases its energy in inelastic scattering. The main difficulties encountered in performing SEM metrology are associated with the mechanism of image formation, when images are formed in the course of electron beam scanning over the surface of the object and represent the sum of sequential responses (from secondary and backscattered electrons) generated by the object in response to inelastic scattering of electrons of an illuminating beam (probe) (the probe is a cross section of the electron beam by the surface of the object). The intensity profiles in SEM images depend on the energy of electrons in the illuminating beam, the probe size, the material of the object and its relief; they reflect the probability distribution of the escape of recoil electrons from different points [16–17]. As a result, the intensity profiles have the shape of curves on which points corresponding to the edges of the object cannot be determined, i.e., the sizes of the object cannot be directly measured. The SEM image is not a copy of the object but is merely its analogue. Therefore, in order to measure sizes of an object with a scanning electron microscope, it is recommended to use an approach based on the simulation of SEM images. This approach involves Monte Carlo calculations of the probabilistic cascade of collisions upon injection of a single electron into the object (and, correspondingly, the escape of recoil electrons) as a function of the energy of this electron and the atomic number of the material under investigation, the averaging/summation of the results and subsequent fitting of the calculated curve to the experimental curve by varying the sizes of the object (the profile fitting method) [16].

The above approach underlies the modern SEM metrology [18] and makes it possible to change over from the image of a reference sample with the known habit and composition [16–17], to the image of a structure that has a similar habit and is formed by another chemical element or an alloy with a homogeneous composition. This approach has been successfully used for measuring sizes of objects with a rectangular or trapezoidal vertical cross section. However, like any approach based on modelling, it depends on the adequacy of the chosen model and is difficult to apply to objects for which their habits and/or distributions of the scattering material are not known exactly a priori. In scanning electron

microscopy, the determination of the habit is based on stereoscopic methods. However, a change in the orientation of the object leads to a change not only in its projection but also in the yield of recoil electrons. Changes in the images of nano-objects due to variations in this yield are comparable to the changes caused by the changes in the projections; consequently, the determination of the habit of the nano-object also presents some problems [16, 19].

The "model" approach is based on two assumptions. First, each electron is scattered independently of other electrons [19], which is equivalent to the independence of the image of each volume with the sizes determined by the sizes of the probe. Second, the image is completely determined by the stage of generation of recoil electrons, i.e., by the corpuscular properties of particles, whereas the role of the process based on the wave properties of an electron is reduced only to changes in the sizes of the probe. When the illuminating electron beam scans the surface of a relief object, the probe becomes alternately farther and closer to the focusing plane, and its sizes change, i.e., defocusings arise [20]. As a result, the object affects the parameters of the probe. However, in the framework of the model approach, it has been postulated that the sizes of a probe during its motion over the surface of a three-dimensional object remain unchanged. This assumption agrees satisfactorily with the modern practice of scanning electron microscopy that operates with images for which the angle of convergence of illuminating electron beams is approximately equal to 10^{-3} rad and the depth of the focus exceeds 1 μm, i.e., in the majority of cases, it exceeds the height of the object [16–17]. The situation radically changes with an increase in the angle of convergence. When the angle of convergence reaches approximately 10^{-1} rad, the depth of the focus becomes equal to or less than 10 nm, which gives rise to noticeable defocusings even for objects with a height of 10÷20 nm. These defocusings (in contrast to the instrumental defocusings associated with the operation of the microscope) can be referred to as the habit defocusings.

Backscattered and secondary electron images exhibit specific features and are differently affected by defocusings. However, in the present paper, these features are not described. We consider only the general regularities of habit defocusings and the possibilities of their use for purposes of metrology. The figure describing the habit defocusings is termed the "action surface," and its cross section along a certain direction is called the "action curve" [20]. The action surface and the action curve uniquely reflect the shape of an object and can be used in measuring the object sizes. In this paper, we consider the approach with the use of action curves, but the results obtained and the recommendations elaborated here can be generalized to the action surfaces.

The action curve is described by the following expression [20]:

$$I_{\Sigma} = \int_{X} \frac{J}{\sqrt{\pi}\sigma} \exp\left(-\frac{(x - x_c)^2}{\sigma^2}\right) dx_c \,. \tag{1}$$

Here, in the linear approximation,

$$\sigma = |z - f| \frac{R - r}{f} + r \,, \tag{2}$$

I_{Σ} is the intensity profile, x_c is the coordinate of the centre of the probe, J is the total intensity of the probe, σ is the root-mean-square deviation (the quantity characterizing the size of the probe), z is the distance from the point on the surface of the object to the output diaphragm of the objective lens, f is the focal length, r is the size of the cross section of the electron beam by the focusing plane, R is the size of the exit aperture of the objective lens, $|z - f|$ is the distance from the point on the surface of the object to the focusing plane, σ corresponds to a particular point on the surface of the object and the region of integration X is determined by the lateral size of the object along the specified direction.

Expression (1) accounts for both the defocusing associated with the object shape, which is responsible for the different distances from the object points at different heights to the focusing plane, and the instrumental defocusing caused by the change in the performance of the optical system. The properties of the action curve can be determined by analysing the regularities of the SEM images with inclusion of the habit defocusing. This treatment can be performed using expression (1), which, in the general case, should be analysed numerically. However, for objects with a rectangular or trapezoidal cross section, this expression can be subjected to an analytical treatment.

If the escape of recoil electrons through the lateral surface of the object is excluded from our consideration, the integration of expression (1) over x_c for the object with a rectangular cross section gives

$$I_X = J_2 + \frac{J_1}{4}\left[\operatorname{erf}\left(\frac{x - x_2}{\sigma_1}\right) - \operatorname{erf}\left(\frac{x - x_1}{\sigma_1}\right)\right], \tag{3}$$

where I_X is the total response at the point with the coordinate x, x_1 and x_2 are the coordinates of the points at the edges of the object, J_1 is the total intensity of the responses from the sample, σ_1 is the root-mean-square deviation from the point inside the object and J_2 is the total intensity of the point of the sample outside the object.

Let us introduce the conditions according to which the probe located at one object/substrate interface should not be superimposed on the probe located at the opposite interface:

$$x = x_2, \qquad (x_2 - x_1) \gg \sigma.$$

Under these conditions, expression (3) at the edge of the object transforms into the expression

$$I_x = J_2 + \frac{J_1}{4}[0-1][(-1)-1] - \frac{J_2}{4}[0-1][(-1)-1] = \\ = J_2 + \frac{J_1}{2} - \frac{J_2}{2} = \frac{J_1 + J_2}{2} \quad . \quad (4)$$

Expression (4) reflects the simple situation: the intensity in the vicinity of the object/substrate interface is determined by the superposition of signals emitted by regions on both sides of the interface in accordance with the intensities of the probe fractions incident on these regions. It follows from expression (4) that all action curves corresponding to different instrumental defocusings intersect each other at the edges of the object at its half-height. During the motion along the line passing through the intersection points, the escape from the object occurs and, after these points are passed, the responses cannot be formed. The image profiles for instrumental defocusings also intersect in the vicinity of these points [21]. However, these profiles account not only for the action curve but also for the regularities of the escape of recoil electrons and, therefore, only approximately reflect the sizes of the object.

4. Determination of the differential profiles, their properties and possibilities of their use in the metrology of nano-objects

Information on the action curve is provided by the images formed under the conditions where the depth of the focus is smaller than the height of the object. The intensity distributions for these images can be described as the sum of two components. The first component is a distribution that is independent of the convergence of the illuminating electron beam and, hence, does not reflect the shape of the object. The second component is determined by the changes in the sizes of the probe during its motion over the surface of the object, i.e., by the habit defocusing. Therefore, in order to determine the component dependent on the habit defocusing, the component independent of the convergence of the illuminating electron beam should be eliminated from the total distribution. There are two techniques used for performing this operation (they are illustrated in Figs. 1 and 2).

In Fig. 1, scheme (1) reflects the specific features of the image formation at a small angle of convergence of the illuminating beam (at a focus depth larger than the object height) and scheme (2) reflects the specific features of the image formation at a large angle of convergence of the illuminating beam (at a focus depth smaller than the object height). In both schemes, the zero-height plane of the object is brought into coincidence with the '**a**' plane onto which the beam is focused. The sizes of the cross sections of the illuminating beam by the zero-height plane of the object (d_{11} and d_{21}) are identical, but the probe sizes (d_{12} and d_{22}) are different, so that the subtraction of the first profile from the second profile gives the differential profile corresponding to $d_{22} - d_{21}$. The first technique can also be implemented using defocused images under the condition where the sizes of the cross sections of the beam by the '**a**' and '**a***' planes are identical, which is provided by focusing onto the '**b**' and '**b***' planes or the '**c**' and '**c***' planes. The defocusing planes '**b**' and '**b***' or '**c**' and '**c***' are separated from the '**a**' and '**a***' planes by different distances ($h_{11} \gg h_{12}$ and $h_{21} \gg h_{22}$), but these distances are chosen so that the sizes of the cross sections of the illuminating beam by the '**a**' and '**a***' planes are identical, which is reflected by the equalities $\xi_{11} = \xi_{21}$ and $\xi_{21} = \xi_{22}$.

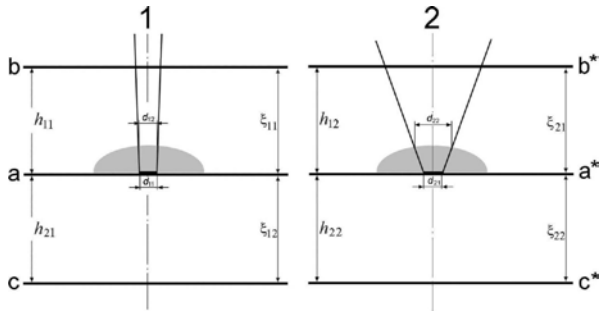

Figure 1. Schemes illustrating the specific features of the implementation of the first technique.

In Fig. 2, scheme (1) reflects the specific features of the image formation in the case where the beam is focused onto two equidistant planes ('**b**' and '**c**') and the zero-height plane of the object is brought into coincidence with the central plane ('**a**'). The scheme (2) reflects the specific features of the image formation in the case where the zero-height plane of the object lies in equidistant planes ('**b**' and '**c**') and the beam is focused onto the central plane ('**a**'). In both schemes, h_1 is the distance between the '**a**' and '**b**' planes, and h_2 is the distance between the '**a**' and '**c**' planes (h_1 and h_2 are identical distances due to changes in the sizes of the cross sections of the illuminating beam).

Designations in scheme (1): 1 and 1* are the generatrices of the cone of rays in focusing onto the **b** plane; 2 and 2* are the generatrices of the cone of rays in focusing onto the **c** plane; d_1 is the size of the cross section of the beam by the **b** plane and d_2 is the size of the cross section of the

beam by the **c** plane ($d_1 = d_2$); d_a is the size of the cross section of the beam by the **a** plane, which is identical for both defocusings; Δf_1 is the distance from the top point of the object to the **b** plane and Δf_2 is the distance from the top point of the object to the **c** plane ($\Delta f_1 < \Delta f_2$); d_b is the probe size in focusing onto the **b** plane and d_c is the probe size in focusing onto the **c** plane ($d_b < d_c$).

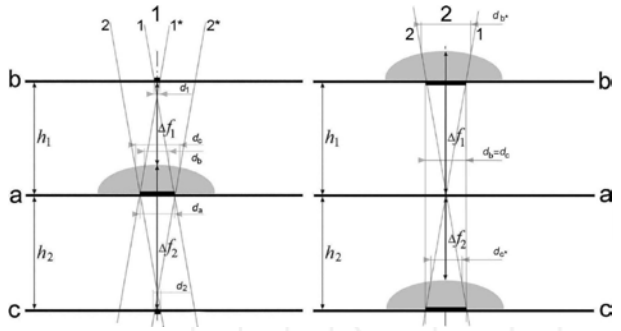

Figure 2. Schemes illustrating the specific features of the implementation of the second technique.

Designations in scheme (2): 1 and 2 are the generatrices of the cone of rays in focusing onto the **a** plane; Δf_1 is the distance between the top point of the object with the zero-height plane in the **b** plane and the focusing plane **a** and Δf_2 is the distance between the top point of the object with the zero-height plane in the **c** plane and the focusing plane **a** ($\Delta f_1 > \Delta f_2$); d_b and d_c are the sizes of the cross sections of the beam by the **b** and **c** planes, respectively (graphically shown) ($d_b = d_c$); and d_{b^*} and d_{c^*} are the probe sizes in the case where the zero-height planes of the object lie in the **b** and **c** planes, respectively ($d_{b^*} > d_{c^*}$).

The first technique is based on the fact that the distribution independent of the convergence of the illuminating beam is also independent of the depth of the focus. According to this technique, the intensity distribution corresponding to the depth of the focus that is many times larger than the height of the object is subtracted from the intensity distribution determined at the depth of the focus that is smaller than the height of the object (Fig. 1). Let us introduce the notion of the zero-height plane of an object, i.e., the plane relative to which the height of the object is measured. A necessary and sufficient condition for the subtraction operation to be realized is the rigorous identity of the sizes of the cross sections of the illuminating beam by the zero-height plane of the object for the two images used (for the image obtained at a larger depth of the focus, this is equivalent to the sizes of the probe). In a specific case, the technique under consideration can be implemented using two images obtained by focusing the beam onto the zero-height plane of the object. However, this technique can also be implemented with the use of the images obtained for instrumental defocusings that are identical in magnitude, i.e., the defocusings for which the sizes of the cross sections of the beam by the zero-height plane of the object during the formation of the compared images are equal to each other. The images obtained under conditions of precision focusings are the most sensitive to the shape of the object, and the defocused images can be used for a detailed examination of the habit.

The second technique is based on the use of two defocused images that correspond to the same sizes of the cross section of the illuminating beam by the zero-height plane of the object and to the defocusings of different signs (Fig. 2). A necessary and sufficient condition for this technique to be realized is the identity of two instrumental defocusings in magnitude. Figure 2 illustrates two variants that ensure this identity. In the first variant, the zero-height plane of the object is brought into coincidence with the central plane and the beam is focused onto two planes that are equidistant with respect to the central plane. In the second variant, two defocused images are formed by means of alternate coincidences of the zero-height plane of the object with two planes that are equidistant with respect to the focusing plane. It should be noted that the equidistance is optical, i.e., the cross sections of the illuminating beam by two profile planes are identical to each other upon focusing onto the central plane, but, upon focusing onto the profile planes, there arise equal cross sections in the central plane irrespective of the plane onto which the beam is focused. Since these two images correspond to the same zero-height plane of the object, the subtraction of one of the relevant intensity distributions from the other distribution also gives rise to a differential profile that depends uniquely only on the habit of the object.

The differential profiles arising in the use of the first and second techniques are described by the expression

$$I_{-} = \int_X \frac{J}{\sqrt{\pi}\sigma_2} \exp\left(-\frac{(x-x_c)^2}{\sigma_2^2}\right) dx_c - \int_X \frac{J}{\sqrt{\pi}\sigma_1} \exp\left(-\frac{(x-x_c)^2}{\sigma_1^2}\right) dx_c , \quad (5)$$

where I_- is the intensity, and σ_1 and σ_2 correspond to the second and first intensity profiles, respectively.

If the quantity σ_i is written in the form $\sigma_0 + \tau$, where σ_0 corresponds to the cross section of the beam by the zero-height plane of the object and τ reflects the changes in the root-mean-square deviation due to the habit defocusing, expression (5) for $|\sigma_0| \gg |\tau|$ in the case where the two profiles used correspond to the same instrumental defocusing σ_0 transforms into the expression

$$I_{-} = \frac{J}{\sqrt{\pi}} \int_{-\infty}^{\infty} \frac{\sigma_2 - \sigma_1}{\sigma_0^2} \left[1 - 2\frac{(x - x_c)^2}{\sigma_0^2} \right] \times \exp\left(-\frac{(x - x_c)^2}{\sigma_0^2} \right) dx_c \quad (6)$$

According to the equality $\sigma_i = \sigma_0 + \tau$, expression (6) for the first technique can be rewritten as

$$I_{-} = \frac{J}{\sqrt{\pi}} \int_{-\infty}^{\infty} \frac{\tau}{\sigma_0^2} \left[1 - 2\frac{(x - x_c)^2}{\sigma_0^2} \right] \exp\left(-\frac{(x - x_c)^2}{\sigma_0^2} \right) dx_c \ . \quad (7a)$$

In the second technique, for each point on the surface, we can write $|\tau_1| = |\tau_2|$, and the quantities τ_1 and τ_2 have different signs depending on the defocusing sign. As a result, expression (6) can be represented in the form

$$I_{-} = \frac{J}{\sqrt{\pi}} \int_{-\infty}^{\infty} \frac{2\tau}{\sigma_0^2} \left[1 - 2\frac{(x - x_c)^2}{\sigma_0^2} \right] \exp\left(-\frac{(x - x_c)^2}{\sigma_0^2} \right) dx_c \ . \quad (7b)$$

In these expressions, the defocusing parameter τ can be replaced by $f(z)$, where z is the displacement of the corresponding point on the surface of the object with respect to the focusing plane; therefore, expressions (6) and (7) can be used for determining the habit of the object.

The intensity distributions reflecting the habit defocusings can also be represented as the sum of two components. The first component is related to the change in the size of the probe according to expressions (1)–(4). The second component is the derivative of the first component, and it accounts for the change in the yield of recoil electrons due to the aforementioned variations in the probe size. The first component affects primarily the resolution, and the average intensity of the detected signal reflecting this component remains unchanged until the probe reaches the edge of the object with a homogeneous composition. However, this signal should change when the probe reaches the edge of the object and its intensity is distributed between the object and the substrate according to expression (4).

In the proposed techniques, it is natural that the substrate surface on which the object is located or formed is chosen as the zero-height plane of the object. In the first technique, the cross section of the illuminating electron beam by the zero-height plane of the object has a size identical to the size of the probe for the image formed at a large depth of the focus and, in the formation of the differential profile, the contribution to the object image due to the scattering from the substrate is eliminated with the first component. In the second technique, both defocused images have the same zero-height plane of the object. This eliminates the contribution of recoil electrons emitted by the substrate to the differential profile. The elimination is especially effective for secondary-electron images for which the response is formed by a thin surface layer and the differential profile reflects only variations in the yield of recoil electrons due to the habit defocusing. However, the elimination also affects the backscattered-electron images in which its efficiency increases with a decrease in the convergence angle of the illuminating beam.

The differential profiles account for the uncorrectable loss of the part of the intensity of the illuminating electron beam in its passage through the contour of the object and the dependence of the yield of recoil electrons, i.e., the differential profiles, in essence, follow the same mechanism of formation as the images arising at a focus depth multiple exceeding the height of the object. However, the differential profile and the intensity distribution in the image formed at a large depth of the focus differ significantly. First, the differential profiles reflect changes in the yield of recoil electrons depending on the habit of the object. Second, the differential profiles are not affected by electrons emitted by the substrate.

The profile of the object along the specified direction can be reconstructed from the differential profile for this direction with the use of the calculation methods based on the inverse integral transformation (matrix inversion) according to expressions (5)–(7) (the habit of the object is reconstructed from the difference surfaces). The accuracy of the determination can be increased by employing the iterative approach with the sequential use of a set of differential profiles corresponding to different instrumental defocusings and/or different techniques used for obtaining the differential profiles. In this case, at each stage, the habit is determined by applying the transformations to the current differential profile with the use of the results obtained at the preceding stages.

The regularities of the formation of the intensity profiles and differential profiles allow for the acquisition of additional information meaning that one can then simplify and refine the results of the above calculations. A number of techniques exist for obtaining this information, and, in some simple cases, the use of these techniques is sufficient for solving metrological problems in the entirety. Let us consider some of these techniques.

Information on the regularities of the change in the height of the object can be obtained by differentiation of the differential profile with respect to z, while information on the changes in the profile of the object along the lateral directions can be obtained by differentiation with respect to x. In combination, these operations enable one to gain an insight into the regularities of the habit of the object.

The yield of recoil electrons drastically increases when the point illuminated by the electron beam comes close to the lateral surface or other face at the distance $l = \Omega/2 + \delta$, where Ω is the size of the probe and δ is the characteristic mean free path in the particular material at the given energy of escape electrons. (A change in the intensity of the escape of recoil electrons can also be stimulated by variations in the composition. The methods used for identifying the factors responsible for the observed changes in the framework of the technique based on the differential profile will be described in the next paper of this series.) Therefore, if the points corresponding to the increase in the escape signal for two compared images are fixed, the distance between these points Δl and the height h of the object is related by the expression $h = \Delta l/(2 \tan \nu)$, where ν is the angle of convergence of the illuminating beam. This approach also makes it possible to estimate the slope of the lateral face (and its crystallographic indices when the plane of projections is determined from diffraction patterns) from the ratio between the measured values of the face height and the length of the face projection. (If the intensity of the incident beam and the sizes of the probe are known, the experimental intensity profiles can be "cleaned of horns" that reflect the escape of recoil electrons near the lateral faces and complicate the operation of the reconstruction of the habit with the use of the inverse integral transformations.) These techniques can also be used to normalize the differential profile of a faceted object and enable one to scale the curves corresponding to the profile of the object. In micrographs, the positions of the points on the surface of the object at which different faces are matched can be determined according to the expression $l = \Omega/2 + \delta$, when the position of the centre at which the yield of recoil electron begins to increase is determined. Similar procedures have been used for studying the habit of objects with a curvilinear surface. However, in this case, the points at which part of the probe goes from the object to the substrate are used as reference points and allowance is made for the fact that probes with different sizes appear on the surface of the object at different distances from its zero-height plane.

From the instant of time when the probe has come close to the lateral surface at a distance equal to the mean free path of electrons with a specified energy, the yield of recoil electrons (intensity) continuously increases as the probe further approaches this surface due to the escape through the two surfaces. However, the yield of recoil electrons begins to decrease after the probe has come into contact with the lateral surface. Therefore, the distance between the maxima of the intensity in two images corresponding to different sizes of the cross sections of the electron beam by the zero-height plane of the object carries information on the sizes of the probes (i.e., on the magnitude of the defocusings).

The differential profiles intersect the zero-height plane of the object at the points lying on the object/substrate interface, i.e., they provide information on the near-bottom region of the object, thus creating conditions for the extraction of information on near-bottom distortions of the object of the specified shape. Points also exist at which differential profiles corresponding to different instrumental defocusings intersect each other. Since the recoil electrons emitted by the substrate do not contribute to the formation of differential profiles, these points lie on its surface and carry information on the lateral sizes of the object.

All the aforementioned points can be used as centres through which the object profiles obtained by the matrix inversion or by fitting of the differential profile should pass.

5. Conclusions: modern scanning electron microscopes and the possibilities of implementing techniques based on differential profiles

One of the conditions providing for the acquisition of reliable data on the sizes and habit of the object is the equidistance of all the points lying on its zero-height plane from the plane of the output diaphragm of the objective lens, which is possible only in the case where the zero-height plane of the object is perpendicular to the optical axis of the instrument. The orientation of the object that ensures this condition became possible owing to the advent of instruments with emitted electron detectors located along the optical axis of the instrument (in-lens SEM), for example, an LEO 1550 VP microscope in which secondary-electron and backscattered-electron detectors are arranged in a similar manner.

Our methods (irrespective of their real incarnation) are based on the use of convergence electron beams. An increase of a convergence of illuminating beam enlarges dramatically the blurring of an illuminated point as a result of the spherical aberration. Possible limitations of the spherical aberration effects (including aberrations associated with large angles of the beam convergence) have been solved in the Hitachi patent [22]. For the implementation of the method, it is necessary to vary the convergence of the illuminating electron beam at precisely specified values. The problem of variation in the angles of convergence is solved by using a two-lens condenser and sets of condenser and objective diaphragms in the Hitachi patent [23].

However, the development of methods of spherical aberration correction and controlled convergence of illuminating beams in scanning electron microscopy is only in its infancy. Therefore, the use of methods

associated with the use of images corresponding to beams with different convergences is difficult especially for small particles. Suggested variants of the method using a sole beam with a limited convergence and based on two defocusings identical in a size, but opposite in signs, is the real alternative to the methods using different convergences. It allows using one convergence, already available in modern microscopes, and realizing the necessary control operations.

The simultaneous processing of the intensity distributions requires the identity (the intensities can be different) (or knowledge) of the intensities of the illuminating beams used for their recording. This problem is also solved for scanning electron microscopes equipped with energy-dispersive X-ray microanalysis systems [24]. In this case, the location of the intensity detector in the plane of the objective lens diaphragms permits one to control the optimization of the shape of the electron beams with the replacement of these diaphragms. The proposed method can also be used to identify the faceting of crystalline objects. For this purpose, it is necessary to determine the crystallographic indices of projections, which can be realized in scanning electron microscopes equipped with detectors for recording Kikuchi maps that arise in electron backscatter diffraction (the EBSD method). These maps make it possible to identify the crystal structure of the object under observation, which is necessary, in particular, to ensure ecological monitoring [11].

The compared profiles should correspond to the same magnifications and the same directions in the object. These problems are solved with software that is installed on computers built into scanning electron microscopes and corrects the operation conditions of the scanning system. It should be noted that the computer support of LEO, Hitachi, JEOL and FEI scanning electron microscopes is sufficient for solving this problem.

The key problem governing the implementation of the proposed approach is to bring the zero-height plane of the object into coincidence with the plane for which the initial sizes of the cross section of the illuminating beam are determined. For objects with nanosizes, these planes must be brought into coincidence with Ångström accuracy. The coincidence of the planes with this accuracy (especially the planes with the a priori unknown relief) cannot be achieved using SEM images. (Particularly stringent requirements are imposed on the coincidence of planes located in regions for which the depth of the focus is less than the height of the object.) Therefore, the planes with which the zero-height plane of the object is brought into coincidence should be built into the system by the manufacturer, and the motion of the object along the axis of the instrument should be terminated at the instant of time when the planes are made coincident with each other. This procedure can be performed using the whole arsenal of development tools that exist in scanning probe microscopy techniques [12]. For example, displacements (especially at the final stage) can be achieved with piezoelectric motors, and the positioning of the object table can be fixed through contacts of the cantilevers with the zero-height plane of the object.

The necessity of performing measurements in the nanoscale range is one of the key problems in nanotechnologies [14, 25]. Among three methods (transmission electron microscopy, scanning probe microscopy and scanning electron microscopy) that have been used for solving metrological problems in the nanoscale range, scanning electron microscopy is the simplest technique, which offers the most illustrative results and does not impose high requirements on the skill of the operators. This method provides the broadest set of magnifications (from $< \times 10$ to $\times 5 \cdot 10^5 \div 1 \cdot 10^6$) and makes it possible to easily change over from one magnification to another, thus retaining specified regions of the object in the field of vision. Scanning electron microscopy is the least demanding in terms of sample preparation and can be non-destructive [16–17]. Modern scanning electron microscopes are equipped with a large number of inbuilt devices, enabling one to control not only the morphology of the object but also its crystal structure, electrophysical characteristics, optical properties, etc. Although the accuracy of measurements decreases because of the noises generated in the signal detection system, the adverse effects of the noises can be reduced by means of improving the detection system and increasing the scan time.

Scanning electron microscopy has remained the most promising candidate to become the key tool for production control in nanotechnologies [14, 26], and the main obstacle to this is the complexity (and, in many cases, impossibility) of the use of SEM images for metrological purposes. Research on the increase in the metrological capabilities of scanning electron microscopes has been performed by all leading manufacturers of these instruments (LEO, Hitachi, JEOL and FEI). The most prominent example of these efforts is provided by the Hitachi microscope in which the pixel of the image system is put in correspondence with the illuminated spot on the surface of the object for the image formation [22]. Although this microscope makes it possible to “draw” the projection of the object with a high accuracy, it does not solve two problems of SEM metrology: (1) the absence of direct relationships between the habit of the object and its image, and (2) distortions of the images due to the superposition of signals (generated by scattering from the substrate) on the intensity profiles of the object.

The proposed method is intended to solve the above problems. This method can be implemented in modern instruments and can be one of the variants of the application of these instruments without the loss of their other capabilities. At the current state of the art in the development of computer technologies, the time required to examine one object is determined by the sum of the times of displacements of the object to the working planes and the times of the recording of intensity profiles. The performance of the operator in implementing the proposed method can be reduced to the insertion of the object into the microscope and the subsequent pressing of buttons that provide changes in the convergence of the illuminating beam, transfer of the object from one plane to another, or the change of the focusing planes, i.e., the complete automation of the measurement process. In this version, the method is especially promising as a tool for production control.

The present paper does not pretend that the proposed method for measuring the sizes of micro- and nano-objects and for determining their habit is ready for practical applications. The microscope community has no experience in comparisons of SEM images that correspond both to different convergences of illuminating beams and to defocusings identical in magnitude, but different in sign, which arise at an insufficient depth of the focus, as the currently available instruments are not suitable for these comparisons. Admittedly, the performed analysis is tentative in character and the habit defocusings were simulated by small instrumental defocusings. Since we were unaware of the magnetic fields penetrating into regions of the location of the objects (most likely, they vary even with changes in the performance of the optical system), the problem was considered in the linear approximation. Undeniably, all these factors will subsequently lead to refinements of the recommendations offered; however, the main conclusion drawn in this paper that it is possible to obtain the intensity distributions, which are sufficient for determining the sizes and habit of the object because they reflect only the object shape, is beyond question.

For the practical implementation of the method, the above systems and components should be built into instruments. Moreover, it is necessary to develop the software that will make it possible to reconstruct the sizes and profile of the object, and to take into account simultaneously the loss of the intensity of the probe due to its motion through the contour of the object and the possibility of escaping recoil electrons through different faces. The solution to this problem will necessitate mental efforts, financial expenses and organization activities. However, without solving the problem of adequate geometric characterization of nano-objects, the further successful and safe (in every respect) development of nanotechnologies is impossible. The purpose of our paper is to call the reader's attention to the fact that there exists a radically new approach in the metrology of micro- and nano-objects, which, in our (possibly, preconceived) opinion, ensures an adequate solution to this metrological problem for the first time. The implementation of the proposed method is associated with certain difficulties. Therefore, this method can be implemented only in the case where its necessity will be recognized by all participants of the nanotechnology community: users of information on the size characteristics of nano-objects (i.e., developers and manufacturers of instruments), providers of information (i.e., metrologists), manufacturers of microscopes and users of nanodevices.

6. References

[1] McNeil SE editor (2011) Characterization of nanoparticles intended for drug delivery. Series: Methods in Molecular Biology, v. 697. Humana Press, 269p.

[2] Goldberg M, Langer R, Jia X (2007) Nanostructured materials for applications in drug delivery and tissue engineering. J. Biomaterials Science, Polymer Edition, 18: 241-268.

[3] Ravichandran R (2010) Physico-chemical evaluation of gymnemic acids nanocrystals. Int. J. Nanoparticles, 3: 280-296.

[4] Lin Y-M, Sun X, Dresselhaus MS (2000) Theoretical investigation of thermoelectric transport properties cylindrical Bi nanowires. Phys. Rev. B, 62: 4610–4623.

[5] Nielsch K, Wehrspohn R, Fisher S, et al. (2001) Magnetic properties of 100 nm nickel nanowire arrays obtained from ordered porous alumina templates. MRS Symp. Proc., 636, D1.9: 1–6.

[6] Thurn-Albrecht T, Schotter J, Kästle GA, et al. (2000) Ultra high density nanowire arrays grown in self-assembled diblock copolymer templates. Science. 290: 2126–2129.

[7] Gudiksen MS, Wang J, Lieber CM (2002) Size-dependent photoluminescence from single indium phosphide nanowires. J. Phys. Chem. B, 106: 4036–4039.

[8] Barnard AS, Yeredla RR, Xu H (2006) Modelling the effect of particle shape on the phase stability of ZrO_2 nanoparticles. Nanotechnology. 17: 3039–3047.

[9] Zapol P, Curtiss LA (2007) Organic molecule adsorption on TiO_2 nanoparticles. A review of computational studies of surface interactions. J. Computational and Theoretical Nanoscience, 4: 222–230.

[10] Zuin S, Pojano G, Marcomini A (2007) Effect-oriented physicochemical characterization of nanomaterials. In Montairo-Riviere N, Tran LC editor. Nanotoxicology. Characterization, dosing and health effects. Informa Healthcare USA Inc. pp. 19–57.

[11] Maksimov SK, Maksimov KS (2009) Controlling the surface functionality of nanomaterials. Nanotechnologies in Russia, 4: 188–200.
[12] Bhushan B, Marti O (2007) Scanning probe microscopy – principle of operation. Instrumentation and Probes. In Bhushan B editor. Springer handbook of nanotechnology, 2nd ed. Berlin, Heidelberg: Springer. pp. 239–278.
[13] Weyland M, Midgley P A (2007) Electron tomography. In Kirkland AI, Hutchison JL, editors. Nanocharacterisation. Cambridge, UK: RSC Publishing. pp. 184–254.
[14] Kirkland AI, Hutchison JL, editors. Nanocharacterisation. Cambridge, UK: RSC Publishing. 316p.
[15] Maksimov SK, Maksimov KS (2009) Principles of nanomaterial control for development of safety standards as illustrated by establishing of laws of nanostructuring in $Ca_yLa_{1-y}F_{3-y}$ and $La_xCa_{1-x}F_{2+x}$ solid solution. Technical Physics Letters. 35: 224–227.
[16] Newbury DE, Joy DC, Echin P, Fiory CE, Goldstein JI (1987) Advanced scanning electron microscopy and X-Ray microanalysis. N.Y., L.: Plenum Press. 454p.
[17] Liu J (2005) High resolution scanning electron microscopy. In Yao N, Wang Zh L editor. Handbook of Microscopy for Nanotechnology. Boston, Dordrecht, N.Y., L.: USA. Kluwer Academic Publishers. pp. 325–360.
[18] Volk Ch P, Gornev ES, Novikov Yu A, et al. (2002). Linear standard of micron, submicron and nanometer diapasons for measurement of sizes of objects with the help of scanning electron and atomic-force microscopes. Microelectronics, 31: 243–262. (In Russian)
[19] Cazaux J (2005) Recent developments and new strategies in scanning electron microscopy. J. Microscopy, 217: 16–35.
[20] Maksimov KS (2009) Regularities of defocused images in scanning electron microscopy and measurements of sizes of nanoobjects. Izvestiya vysshikh uchebnykh zavedenii. Elektronika, No 2: 69–73. (in Russian).
[21] Ilyin MI, Kozlitin AI, Maksimov SK, Nikitin AV, Bannikov VV (1997) High accuracy and precision measurements of sub-0.25-micron and nanometer objects in scanning electron microscopy. Scanning. 19: 224–225.
[22] Kawasaki T, Yoshida Y, Ose H, Todokoro H, (2007) Electron beam apparatus with aberration corrector. US pat. 7,199,365.
[23] Kitsuki H, Aoki K, Sato M (2008) Scanning electron microscope. US pat. 7,442,929.
[24] Zhou W, Wang Z L editor (2005) Scanning microscopy for nanotechnology: Techniques and applications. Boston, Dordrecht, N.Y., L.: Kluwer Academic Publishers. pp. 325–360.
[25] Bhushan B editor (2007) Springer Handbook of Nanotechnology. 2nd ed. Berlin. Heidelberg: Springer. 1916p.
[26] Yao N, Wang ZL editors (2005) Handbook of Microscopy for Nanotechnology. 2nd ed. Berlin. Heidelberg: Springer. 742p.